JOURNAL OF MATERIALS SCIENCE 31 (1996) 6269–6278

Vinylphosphonic acid-modified calcium aluminate and calcium silicate cements

T. SUGAMA
Energy Efficiency and Conservation Division, Department of Applied Science, Brookhaven National Laboratory, Upton, NY 11973, USA

R. N. MORA Jr
Department of Civil Engineering, California State University, Northridge, CA, USA

Cementitious materials in terms of calcium phosphate cements (CPC) were prepared through the acid–base reaction between vinylphosphonic acid (VPA) and calcium aluminate cement (CAC) reactants or calcium silicate cement (CSC) reactants at 25 °C. Using CAC, two factors were responsible for the development of strength in the cements: one is the formation of an amorphous calcium-complexed vinylphosphonate (CCVP) salt phase as the reaction product, and the other was the high exothermic reaction energy. Because the formation of CCVP depletes the calcium in the CAC reactants, $Al_2O_3 \cdot xH_2O$ gel was precipitated as a by-product. CCVP → amorphous calcium pyrophosphate hydrate (CPPH) and $Al_2O_3 \cdot xH_2O \rightarrow \gamma$-AlOOH phase transitions occurred in the CPC body autoclaved at 100 °C. Increasing the temperature to 200 °C promoted the transformation of CPPH into crystalline hydroxyapatite (HOAp). In the VPA–CSC system, the strong alkalinity of CSC reactant with its high CaO content served in forming the CPPH reaction product which led to a quick setting of the CPC at 25 °C. Hydrothermal treatment at 100 °C resulted in the CPPH → HOAp phase transition, which was completed at 300 °C for both the VPA–CAC and VPA–CSC systems, and also precipitated the silica gel as by-product. Although the porosity of the specimens was one of the important factors governing the improvement of strength, a moderately mixed phase of amorphous CPPH and crystalline HOAp as the matrix layers contributed significantly to strengthening of the CPC specimens.

1. Introduction

This paper describes our continuing studies on acid–base reaction cements which have a high potential for use as alkali carbonation-resistant cementing materials to support intermediate casing pipes, and to protect them from corrosive fluids and gases in geothermal wells where temperatures may raise to 300 °C. Previously, we investigated the reaction kinetics and pathways, phase compositions and transformation, and *in situ* microstructure development for the calcium phosphate cements (CPC) consisting of the NH_4- or sodium-containing phosphate compounds as the acid liquid reactants, and calcium aluminate cements (CAC) as the base solid reactants, at room and hydrothermal temperatures, ranging from 25–300 °C [1–3]. Using the NH_4-based phosphate reactants, the rate of reaction with the CAC base reactants depended primarily on the mole fraction of the CaO in the CAC; namely, a high mole fraction resulted in the evolution of greater exothermic reaction heat, reflecting the rapid setting behaviour of CPC. Further, we found that amorphous NH_4 or sodium calcium orthophosphate, NH_4- or Na–$CaPO_4 \cdot xH_2O$ salts, formed by acid–base reactions at an ambient temperature, were responsible for the development of strength. This reaction also led to the formation of $Al_2O_3 \cdot xH_2O$ gel by-products on the surfaces of calcium-depleted CAC reactants. When these amorphous phases, which bind the partially reacted and non-reactive CAC particles into a coherent mass, were autoclaved at 100–300 °C, the occurrence of *in situ* phase transitions, NH_4- or Na–$CaPO_4 \cdot xH_2O \rightarrow$ crystalline hydroxyapatite, $Ca_5(PO_4)_3(OH)$, and $Al_2O_3 \cdot xH_2O \rightarrow$ crystalline boehmite, γ-AlOOH, significantly improved the cement's mechanical strength. Such transformations not only resulted in hydrothermally stable cements, but also served to yield the chemical components in the cements which were unsusceptible to alkali carbonation at elevated temperatures [4].

To date, all the information on the CPCs has been gained using inorganic acid reactants, such as $NH_4H_2PO_4$, NaH_2PO_4, and $-(-NaPO_3-)-_n$, and calcium aluminate base reactants, such as monocalcium aluminate, $CaO \cdot Al_2O_3$ and calcium bialuminate, $CaO \cdot 2Al_2O_3$. Thus, in this work, our particular interest was to employ monomeric vinylphosphonic acid (VPA) which has two chemical components, organic (CH_2=CH) and inorganic [$P(O)(OH)_2$], in its molecular structure, and to use the calcium silicate base

0022–2461

reactants; our aim was to replace the conventional inorganic phosphates and to compare them with the calcium aluminate reactants. Ellis and Wilson [5] investigated cements formed from the reaction between poly(vinylphosphonic acid) (PVPA) and aluminosilicate glasses for use as dental cementing materials. They concluded that their properties, such as setting time and mechanical strength, depended mainly on the Si/Al mole ratios in aluminosilicate structure; namely, a low ratio led to rapid setting and good mechanical behaviour at room temperatures. However, there is no information on the pathway of the chemical interaction between PVPA and aluminosilicate glasses at room temperature, nor is it known what would occur if PVPA-derived cements were exposed to hydrothermal environments at temperatures up to 300 °C, and how the phase composition, microstructure, and mechanical properties of such cements would be changed by the attack of hot water under high pressure.

Based upon the information described above, the emphasis in the present study was directed towards characterizing CPC formed by acid–base reactions between monomeric VPA solutions and calcium aluminate or calcium silicate cement reactants at room temperature, and followed by hydrothermal treatments at temperatures up to 300 °C. The following five characteristics were studied: (1) the extent of the exothermic reaction, (2) the mechanism of interaction, (3) the identification of the reaction products, (4) the phase compositions and transitions, and (5) the development of microstructure. All the information obtained was correlated directly with changes in the porosity and compressive strength of the specimens prepared at 25 °C, and at the hydrothermal temperatures of 100, 200, and 300 °C.

2. Experimental procedure

2.1. Materials

A monomeric vinylphosphonic acid (VPA),

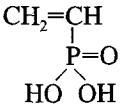

supplied by Hoechst Chemicals, was used as the proton-donating acid reactant. The VPA was dissolved in water to make a 88 wt % solution at pH 1.3. Three solid base reactants; Secar 80 (#80) and Refcon (RE) as calcium aluminate cements (CAC) reactants, and Class G (G) as calcium silicate cement (CSC) reactants, were obtained from the Lafarge Calcium Aluminates, Lehigh Portland Cement Company, and California Portland Cement Company, respectively. The X-ray powder diffraction (XRD) data for the two CAC reactants showed that the major chemical components of #80 consist of monocalcium aluminate ($CaO \cdot Al_2O_3$, CA), calcium bialuminate ($CaO \cdot 2Al_2O_3$, CA_2), and corundum (α-Al_2O_3), while RE has CA and gehlenite ($2CaO \cdot Al_2O_3 \cdot SiO_2$, C_2AS) as its major components, and CA_2 as a minor one. No α-Al_2O_3 phase was identified in RE. In contrast, the main mineralogical component of G was tricalcium silicate ($3CaO \cdot SiO_2$, C_3S).

Neat cement pastes were prepared by thoroughly hand-mixing 60 wt % cement base reactants and 40 wt % VPA solution at room temperature; cement slurries were cast in cylindrical moulds (30 mm diameter × 65 mm long), and allowed to harden at 25 °C in air for 24 h. These specimens, aged for 24 h, were removed from the mould, and then autoclaved for 20 h at temperatures up to 300 °C. The compressive strength and porosity of the hardened specimens were measured as a function of hydrothermal temperature; we also identified the reaction products and phase compositions, and examined the microstructural development to determine what factors were responsible for the improved strength of the neat CPC pastes.

2.2. Measurements

Differential scanning calorimetry (DSC) was used to obtain some kinetic parameters (onset and peak temperatures, and total reaction energy) of the exothermic acid–base reaction between the CAC or CSC and the VPA. Information on the chemical reaction products, and the phase compositions and transitions of CPC before and after autoclaving, was gained using Fourier transform–infrared (FT–IR) and X-ray power diffraction (XRD). An image analysis was made to examine the development of the microstructure and the chemical components of the fractured CPC surfaces, using scanning electron microscopy (SEM) coupled with energy-dispersive X-ray spectrometry (EDX). The porosity of CPC specimens was measured by helium comparison pyconometry. Compressive strength tests were performed on the cylindrical CPC specimens with a diameter of 30 mm and a length of 65 mm; the result given is the average value of three specimens.

3. Results and discussion

3.1. Exothermic acid–base reaction

To obtain data on the degree of reactivity of the VPA reactant with the CAC and CSC base reactants, and on the exothermic energy generated by acid–base reaction between VPA and CAC or CSC, differential scanning calorimetry (DSC) was employed. Using the non-isothermal method at a constant rate of $10\,^{\circ}C\,min^{-1}$ in nitrogen environment, the resulting DSC curve (see Fig. 1) for all samples showed a typical exothermic feature as a function of temperature. The enclosed area, A, of the curve with the baseline represents the total heat evolved during the exothermic reaction. Thus, the exothermic energy, ΔH ($mcal\,mg^{-1}$), can be computed using the formula, [6, 7]

$$\Delta H = TRA/hm \qquad (1)$$

where T, R, A, h and m refer to the temperature scale ($^{\circ}C\,in^{-1}$), the range sensitivity ($mcal\,s^{-1}\,in^{-1}$), the peak area (in^2), the heating rate ($^{\circ}C\,s^{-1}$), and the sample's weight (mg), respectively. Also, we determined the two temperatures at which the DSC

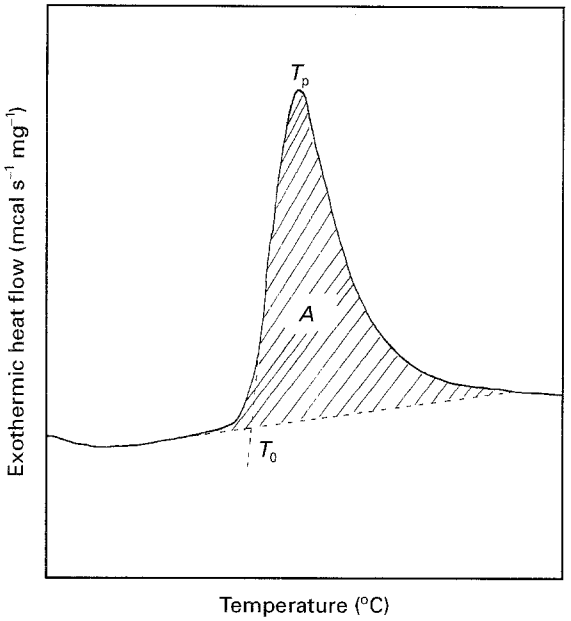

Figure 1 Non-isothermal DSC curve showing the total acid–base reaction energy.

TABLE I Reaction parameters for #80-, RE-, and G-VPA systems

System	Onset temperature, T_0 (°C)	Peak temperature, T_p (°C)	Total exothermic energy, ΔH (mcal mg^{-1})
#80	42.5	51.5	2.56
RE	20.5	40.2	7.85
G	7.2	16.5	2.78

curves show the onset, T_0, and peak, T_p, of the exothermic reaction; the former, T_0, was estimated from the curves by finding the intersection point of two linear extrapolations. Table I compares such reaction parameters of #80-, RE-, and G–VPA cement systems. In this experiment, the two components, acid and base reactants, were separately left for ≈ 10 h in the refrigerator at ≈ 3 °C, before mixing them. As shown, the onset, T_0, and peak, T_p, temperatures of exothermal reaction depended primarily on the base reactants; namely, incorporating the G reactant gave the lowest onset and peak temperatures of 7.2 and 16.5 °C, respectively. When RE was used, the onset and peak positions shifted to the high-temperature side. A further shift to the high-temperature side was recorded from the #80 system. As a result, the extent of reactivity of base reactants to VPA has the following order: G > RE > #80.

On the other hand, the comparison between the values of ΔH evaluated by the acid–base reaction demonstrated that the highest ΔH of 7.85 mcal mg^{-1} was obtained from the RE system. The G system generated the second highest value, although it was $\approx 35\%$ lower than that of the RE system. Our attention was directed next to better understanding of why the G reactant has the strongest attraction to the acid reactants, and why the RE system evolves a high ΔH. The major chemical ingredients of these base reactants consisted of CA, CA_2, and α-Al_2O_3 phases for #80, CA and C_2AS phases for RE, and the C_3S phase for G. Thus, we again investigated such reaction parameters on the DSC curves generated from the reaction between the VPA and the respective base components (CA_2, CA, and C_3S). As shown in Table II, the data clearly demonstrated that the changes in T_0 and T_p values related directly to the mole fraction of CaO in the base reactants; an increase in the mole fraction of CaO resulted in a decrease in T_0 and T_p temperatures. Hence, the ranking of the reactivity of these chemical components was $C_3S > CA > CA_2$, embodying the fact why the G reactant containing the C_3S as its major phase contributed significantly to its greater reactivity with the acid reactants. In contrast, the #80 reactant with CA_2 as one of its major phases has a poor chemical reactivity with the VPA. The data also showed that the most effective component in generating a high ΔH was the CA phase, whereas the CA_2 phase had the lowest ΔH. Because one of the major components for the RE and #80 reactants is CA and CA_2, respectively, this information corresponded to that obtained from the CAC and CSC reactants–VPA systems (Table I); namely, the increase in ΔH value was in the order; RE > G > #80. Furthermore, these reactive parameters were correlated with the difference in porosity and compressive strength for the #80-, RE-, and G-VPA cement pastes at 3 h after mixing at 25 °C. The specimens with the porosity of $< 40\%$ can be made from the use of RE reactant. By contrast, the pastes made from the #80 system had the porous structure, with a porosity of $> 50\%$. Although both the acid and base components were cooled to 3 °C, the G system promptly set after mixing the components, so that it was very difficult to case the mixture in the moulds. Hence, there was no information on its porosity and compressive strength. The values for porosity and compressive strength of these specimens were as follows: a 53.3% porosity and 0.23 MPa compressive strength for the #80 system,

TABLE II Reaction parameters for CA_2-, CA-, and C_3S–VPA systems

System	Mole fraction			Onset temperature, T_0 (°C)	Peak temperature, T_p (°C)	Total exothermic energy, ΔH (mcal mg^{-1})
	CaO	Al_2O_3	SiO_2			
CA_2	0.22	0.78	0.00	58.4	75.1	9.31
CA	0.34	0.65	0.00	30.4	40.2	20.60
C_3S	0.74	0.00	0.26	14.4	22.7	12.26

and a 37.6% porosity and 3.79 MPa compressive strength for the RE system. As expected, an increase in porosity of cement pastes was related directly to a lowering of compressive strength. Moreover, it is likely that the ΔH value is a major factor which contributes to strengthening the pastes, along with the development of a dense cement structure. In fact, the high ΔH generated in the RE system was responsible for the increase in strength.

3.2. Reaction products at 25 °C

To identify the reaction products formed in the 25 °C/3 h aged cement bodies, we investigated the FT–IR absorption bands of powdered samples over the two frequency ranges, 4000–2500 and 1400–600 cm^{-1}. The IR spectra of individual reactants also were inspected as the reference bands. Fig. 2 shows the spectra for the VPA and #80 reference reactants, and the VPA-#80 cement sample. A typical spectrum of VPA liquid has a broad absorption band near 2867 cm^{-1}, which can be ascribed to the CH stretching frequency in unsaturated vinyl groups ($=CH_2$ and $=CH$), and P–O–H stretching in phosphonic acid; a band at 1261 cm^{-1}, revealing the stretching of P=O double bonds; one at 955 cm^{-1}, belonging to the P–O–H bending mode in phosphonic acid; and also a band at 781 cm^{-1} corresponding to the stretching mode of C=C double bonds. The IR spectrum of #80 reactant showed that non-reacted #80 powders have already been partially hydrated because of the presence of the peaks at 3530 and 3460 cm^{-1}, reflecting an O–H stretching vibration in H_2O. When the #80 was incorporated into the VPA, the particular feature of its IR spectrum, compared with those of the VPA and #80 reference samples, was the appearance of new bands at 3378 and 1085 cm^{-1}, in addition to all of the bands, corresponding to the VPA and #80 reactants. A possible assignment of the former new band is due to the new hydration products yielded by the reaction between VPA and #80. The latter strong band can be accounted for by P–O stretching in ionic phosphonate groups [8, 9], such as PO_3^{2-} and HPO_3^-. If this interpretation is correct, then phosphonate complexes may be formed by the acid–base reaction between #80 and VPA. These hypothetical complexes are illustrated below (II and III).

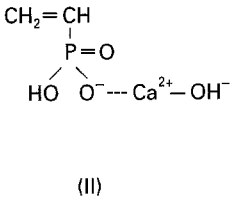

(II)

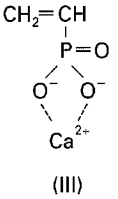

(III)

These complex structures may be formed by the following reaction route; when the surfaces of #80 grains, acting as a cation-leaching base powder, come into contact with VPA as a proton-donating acid liquor, protons released from the VPA increasingly promote the liberation of calcium cations from the

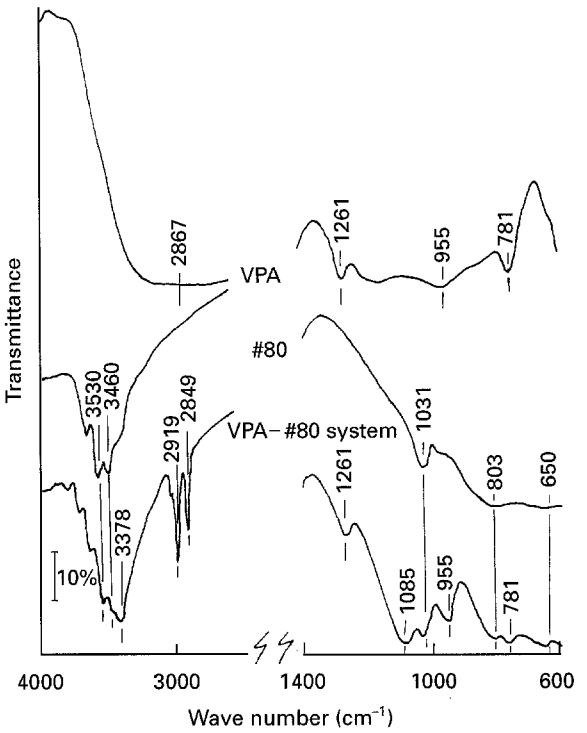

Figure 2 FT–IR spectra for VPA and #80 reference samples and VPA–#80 system made at 25 °C.

binary phases, such as CA and CA_2, in generic acid–base reaction processes. As described in our previous paper [2], the dissociation of a large amount of Ca^{2+} causes the phase segregation of CA and CA_2, thereby forming an $Al_2O_3 \cdot xH_2O$ gel as the by-product from the calcium-depleted #80 grains. The uptake of calcium cations by the phosphonate anions perhaps generates calcium-complexed vinyl phosphonate (CCVP) salts and half-salts as the major reaction products. The latter salts have the Ca^{2+} linked to OH^-. Assuming that such a reaction occurs in the mixture of VPA and #80, the hydrate-related new band at 3378 cm^{-1} is attributable to the $Al_2O_3 \cdot xH_2O$ by-product. The spectrum also indicated that some non-reacted #80 cement reactant still remained in the matrix phases consisting of CCVP salts and $Al_2O_3 \cdot H_2O$ gel. Nevertheless, this matrix phase which binds the partially reacted and non-reactive #80 particles, appears to be responsible for the development of the strength of cement pastes. Reaction products similar to those of the #80 system were identified in the RE system at 25 °C (IR spectra not shown). However, a striking difference in spectral features was detected from the rapid-setting G system, (Fig. 3). The differences were as follows: (1) the elimination of the absorption bands at 2867 and 781 cm^{-1} originating from the unsaturated vinyl groups in the VPA, (2) a significant decrease in intensity and the disappearance of the G-related peaks, and (3) the emergence of new sharp bands at 3330, 1108, 1038, 991, and 744 cm^{-1}. The four new bands at 1108, 1038, 991 and 744 cm^{-1} are assignable to the formation of pyrophosphate [10]; the first three bands correspond to the P–O and P–O–P stretching modes in the P–O–P linkages, and the last band at 744 cm^{-1} is due

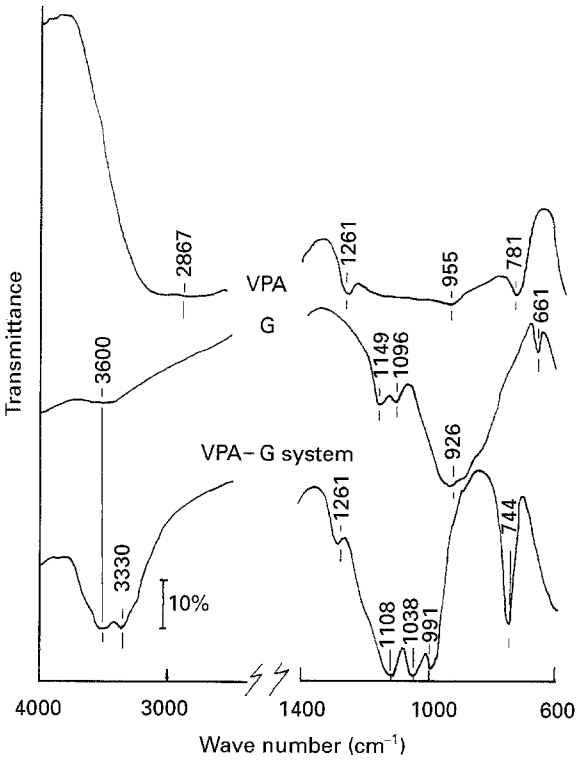

Figure 3 FT–IR spectra for VPA and G reference samples and 25 °C made VPA–G system.

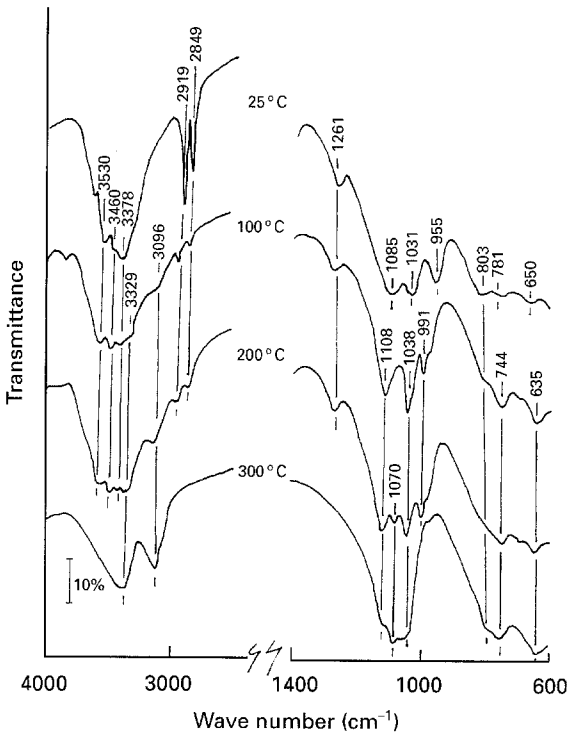

Figure 4 FT–IR spectra for VPA–#80 systems at 25 °C, and autoclaved at 100, 200, and 300 °C.

to P–O–P bending. The other new frequency at 3330 cm^{-1} is due to the OH groups in the pyrophosphate-related hydrates. Relating this finding to difference 1, the results seem to suggest that the vinyl groups in VPA are vulnerable to the attack of the G reactant. In the other words, the activity of the strong alkali-inducible G reactant not only contributes to the rapid setting of the pastes, but also promotes bond breakage of the vinyl groups in VPA. Such a disintegration might transform phosphonic acid into pyrophosphate, reflecting the introduction of calcium pyrophosphate hydrate (CPPH), $CaH_2P_2O_7 \cdot xH_2O$, in the cement body. To support this interpretation, the alkalinity of all the base reactants was estimated by comparing the pHs of the interstitial fluids of cement slurries extracted by centrifugation; we used the slurries consisting of 50 g cement and 50 g water, left for 3 min at 25 °C after mixing. The pH values of G, RE, and #80 cement slurries were 12.01, 10.81, and 10.21, respectively. Thus, the G cement is the most reactive base reactant to VPA in the acid–base reaction processes. Also, its strong alkalinity promotes the disintegration of vinyl groups.

The FT–IR information was correlated directly with data obtained from XRD analyses of the same samples. XRD patterns (not shown) for the #80, RE, and G samples made at 25 °C showed that all the reaction products and by-products were essentially in an amorphous phase; namely, XRD tracings, from 0.39–0.24 nm, indicated only the presence of nonreacted components, such as CA, CA_2, and α-Al_2O_3 phases for the #80 reactant, CA, C_2AS and CA_2 for the RE reactant, and C_3S for the G reactant.

3.3. Hydrothermally treated cements

Next, our emphasis was upon identifying subsequent *in situ* phase transformations and compositions, and the development of microstructure for the #80-, RE-, and G–VPA cement systems after exposure for 20 h in an autoclave at 100, 200, and 300 °C. We used FT–IR, XRD, and SEM–EDX analyses. The information from these experiments then was correlated directly with the porosity and compressive strength of the 100, 200, and 300 °C/20 h autoclaved specimens.

Fig. 4 shows FT–IR spectra for the #80 system autoclaved at 100, 200, 300 °C for 20 h. For comparison with those of the autoclaved cements, the spectrum of the 25 °C made sample is also included in the figure. When the 25 °C sample was hydrothermally treated at 100 °C, the spectrum showed the three noticeable differences: (1) the development of new bands at 3329, 3096, 1108, 1038, 991, 744, and 635 cm^{-1}, (2) a considerable reduction in the intensity of the unsaturated vinyl group- and #80-related bands, and (3) the loss of the phosphonate band at 1085 cm^{-1} developed by the acid–base reaction at 25 °C. Regarding difference 1, the typical bands reflecting the formation of boehmite, γ-AlOOH, are identical at the frequency positions of 3329, 3096, 744, and 635 cm^{-1} [11, 12]. Hence, the bands at 3329 and 3096 cm^{-1} are attributable to the O–H stretching in the γ-AlOOH, and the frequencies at 744 and 635 cm^{-1} are due to the stretching of the Al–O linkage in γ-AlOOH. The other new bands correspond to pyrophosphate groups formed by the hydrothermally catalysed transformation of phosphonate groups. Because the creation of pyrophosphate is related to the formation of CPPH, it is reasonable to believe that the bands near 3330 and 744 cm^{-1} not only represent the O–H and Al–O

stretching in γ-AlOOH, but also belong to the O–H stretching and P–O–P bending vibrations in the CPPH. These findings are correlated directly with the results of differences 2 and 3. Clear evidence for this conclusion was the fact that the transitions of two phases occur at the hydrothermal temperature of 100 °C; one transition was the conversion of the $Al_2O_3 \cdot xH_2O$ gel formed by the phase segregation from CA and CA_2 in the #80 reactant at 25 °C, into γ-AlOOH and the other was the *in situ* CCVP → CPPH transformation. From the increase in intensity of the γ-AlOOH-related bands, it is apparent that exposure to 200 °C further promotes an increase in the rate of the $Al_2O_3 \cdot xH_2O \rightarrow$ γ-AlOOH phase transition. Considerable attention in the spectrum at 200 °C was paid to the development of additional band at 1070 cm^{-1}, revealing the P–O stretching of the hydroxyapatite, $Ca_5(PO_4)_3(OH)$, (HOAp) [1], while the intensity of vinyl group-related bands became very weak. Hence, HOAp seems to be formed by the hydrothermally catalysed phase transition of CPPH at temperatures near 200 °C. As seen in the spectrum at 300 °C, the rates of $Al_2O_3 \cdot xH_2O \rightarrow$ γ-AlOOH and CPPH → HOAp transitions are accelerated increasingly; the bands related to γ-AlOOH and HOAp became the predominant peaks, thereby resulting in a noticeable decrease in the intensity of the non-reacted #80- and CPPH-related bands. In addition, the vinyl– and P=O-related bands were hardly recognizable in this spectrum. The disappearance of P=O groups at 1261 cm^{-1} peak demonstrates that HOAp has a tetrahedral phosphate structure formed by the rupture of P=O bonds in CPPH. Also, we note that the band at 803 cm^{-1}, present over a wide temperature range from 25–300 °C, may be due to α-Al_2O_3 [12] which is one of the chemical components in the #80 reactant. For the RE system, the changes in spectral feature as a function of temperature were similar to those of the #80 system (data not shown).

In the G system (Fig. 5), compared with that of 25 °C, the only difference in spectral features at 100 °C was that the shape of the peak, ranging from 1110–900 cm^{-1}, became much wider, suggesting that an additional peak develops at a frequency position of 1070 cm^{-1}, corresponding to the formation of HOAp. However, we assume that this new band is not only assigned to the HOAp, but also may be due to the formation of silica gel, $(SiO_2)_n \cdot xH_2O$ [13]. If this assignment is correct, the calcium-depleted G reactants brought about by the precipitation of HOAp and CPPH may be converted into the silica gel as by-product. At 200 °C, there is no change in the major chemical components of cements. Hence, the phase composition of the matrix formed at 100 and 200 °C appears to consist of CPPH, HOAp, and silica gel. Increasing the temperature to 300 °C intensified the shoulder band at 1070 cm^{-1}, implying that well-formed HOAp and silica gel can be produced at 300 °C. In addition, a new band was created around 3450 cm^{-1}, while the intensity of the bands at 3600, 3330, and 744 cm^{-1}, belonging to the partially hydrated G reactants and CPPH, and the P=O band at 1261 cm^{-1} were significantly reduced or vanished.

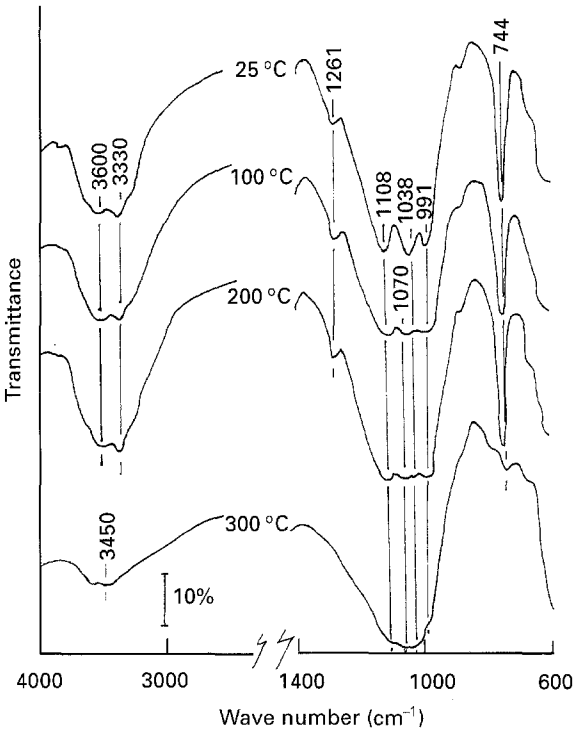

Figure 5 FT–IR spectra for the VPA–G system at 25 °C, and autoclaved at 100, 200, and 300 °C.

This new frequency at 3450 cm^{-1} possibly can be assigned to the OH band in HOAp and silica gel.

This information was supported by XRD analyses, using the same specimens as those used in the FT–IR study. The XRD results from these powder samples are given in Figs 6–8. For the #80 systems (Fig. 6), the diffraction pattern of the 100 °C autoclaved samples showed the presence of crystalline γ-AlOOH as the by-product, in conjunction with non-reacted CA, CA_2 and α-Al_2O_3 as the chemical components of #80 cement. At 200 °C, the following changes can be seen: the introduction of an additional crystalline phase, HOAp; an increase in the line intensities of γ-AlOOH; and, attenuation of the CA- and CA_2-related peaks. As expected, increasing the hydrothermal temperature to 300 °C led to a well-formed HOAp together with γ-AlOOH phase, and the residual CA and CA_2 reactant-related spacings had diminished, while an intense line of α-Al_2O_3 still remains. Thus, the reactivity of α-Al_2O_3 with VPA appears to be poor. For the RE specimens autoclaved at the same temperatures (Fig. 7), the pattern at 100 °C had a strong line intensity for the C_2AS and CA reactants as the major phases, and a lesser intensity for the CA_2 reactant and γ-AlOOH. An interesting alteration in XRD pattern with temperature was seen in the 200 °C autoclaved RE specimens; the C_2AS reactant was existent as an intense line, while the intensities of the CA- and CA_2-related lines are markedly reduced. This finding strongly verified that the CA and CA_2 preferentially reacted with VPA, rather than C_2AS. Nevertheless, the amorphous $Al_2O_3 \cdot xH_2O$ gels formed as by-products of the acid–base reaction between CA or CA_2 and VPA at 25 °C were converted into γ-AlOOH under hydrothermal conditions. The pattern also showed that this hydrothermal temperature contributed to

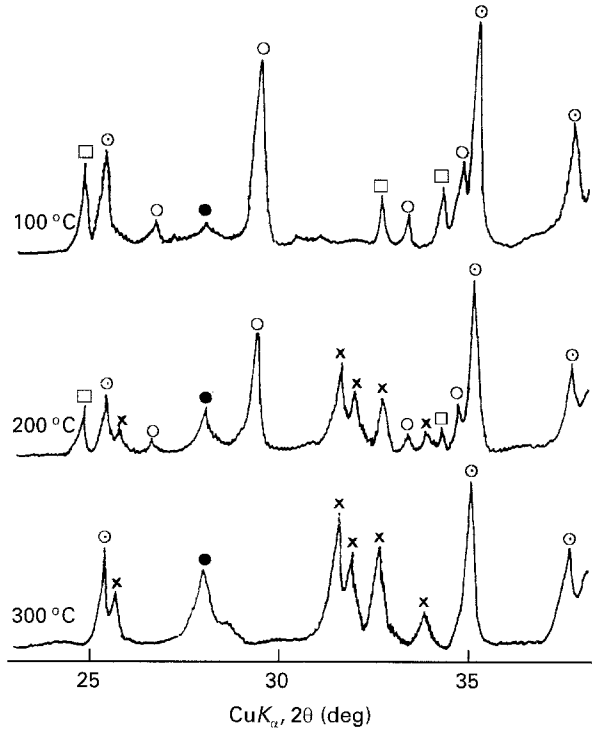

Figure 6 Comparison between XRD patterns for 100, 200, and 300 °C autoclaved VPA–#80 systems. (○) CA, (□) CA_2, (⊙) α-Al_2O_3, (●) γ-AlOOH, (×) HOAp.

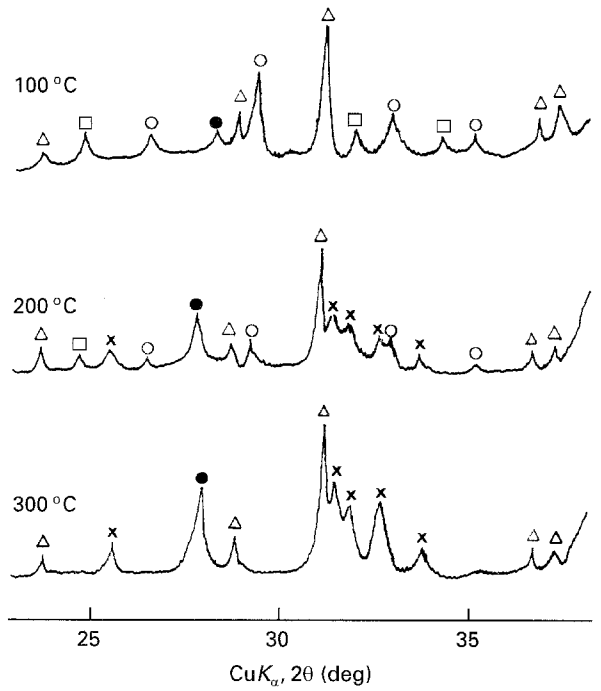

Figure 7 XRD tracings of 100, 200, and 300 °C autoclaved VPA–RE specimens. (○) CA, (□) CA_2, (△) C_2AS, (●) γ-AlOOH, (×) HOAp.

developing some HOAp phase. As shown in Fig. 7, the HOAp phase eventually became the major component, when the RE specimens were autoclaved at 300 °C. However, a certain amount of C_2AS reactant still remains in the cement. In contrast, the CA and CA_2 reactants were entirely eliminated at this temperature. In autoclaved G systems (Fig. 8), exposure at 100 °C contributed to introducing HOAp as the minor

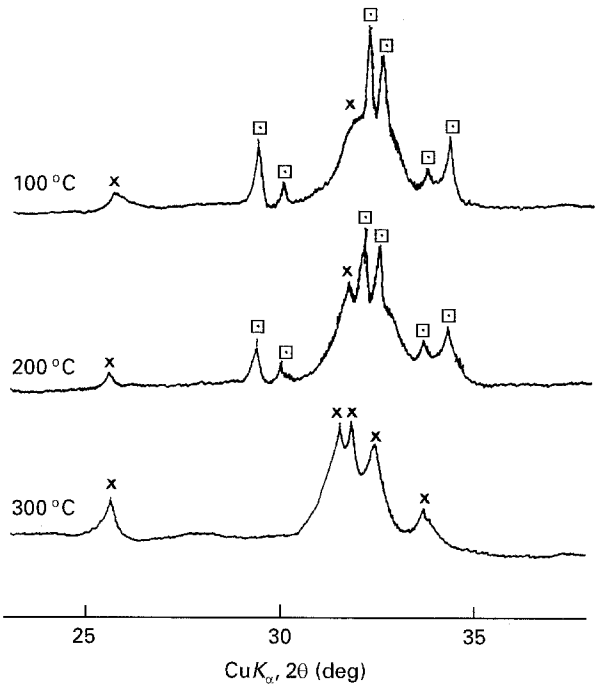

Figure 8 XRD patterns for 100, 200, and 300 °C autoclaved VPA–G systems. (⊡) C_3S, (×) HOAp.

phase in the CPPH amorphous matrix, suggesting that this information corresponds to that obtained from the FT–IR data. The *d*-spacings also showed that the non-reacted C_3S reactant remained as the major component of G cement in 100 °C autoclaved specimens. At 200 °C, the features of the XRD pattern closely resembled those from specimens at 100 °C. However, increasing the temperature to 300 °C significantly intensified the line of HOAp, implying that HOAp had become the major phase, while all the C_3S-related *d*-spacings were eliminated. No crystalline SiO_2 compounds were found in these patterns.

Fig. 9 shows the scanning electron micrographs together with the EDX spectra of fractured surfaces from VPA–RE specimens autoclaved at 100 and 300 °C. At 100 °C (Fig. 9a), the morphological features were expressed as a rough surface texture containing a large number of voids of ≈ 1 μm. The EDX spectrum of the area, denoted as site A, represents its chemical composition consisting of oxygen, aluminium, silicon, phosphorus and calcium, reflecting the presence of hybrid phases, such as CPPH, $Al_2O_3 \cdot xH_2O$, CA, C_2AS, CA_2 and γ-AlOOH. Thus, a possible interpretation of this SEM image is the composite structure of an amorphous CPPH matrix, which binds the partially reacted and unreactive RE particles, and the $Al_2O_3 \cdot xH_2O$ and γ-AlOOH by-products, into a coherent mass. A striking change in microtexture was observed in the SEM micrographs of 300 °C autoclaved specimens (Fig. 9b) that disclosed growths of plate-like crystals. The EDX spectrum of area B had a strong line intensity of phosphorus and calcium as dominant elements, moderate intensity of oxygen and aluminium peaks, and a weak silicon signal. Hence, these crystals seem to represent a hybrid structure, consisting of the HOAp as principal crystal component, and the γ-AlOOH

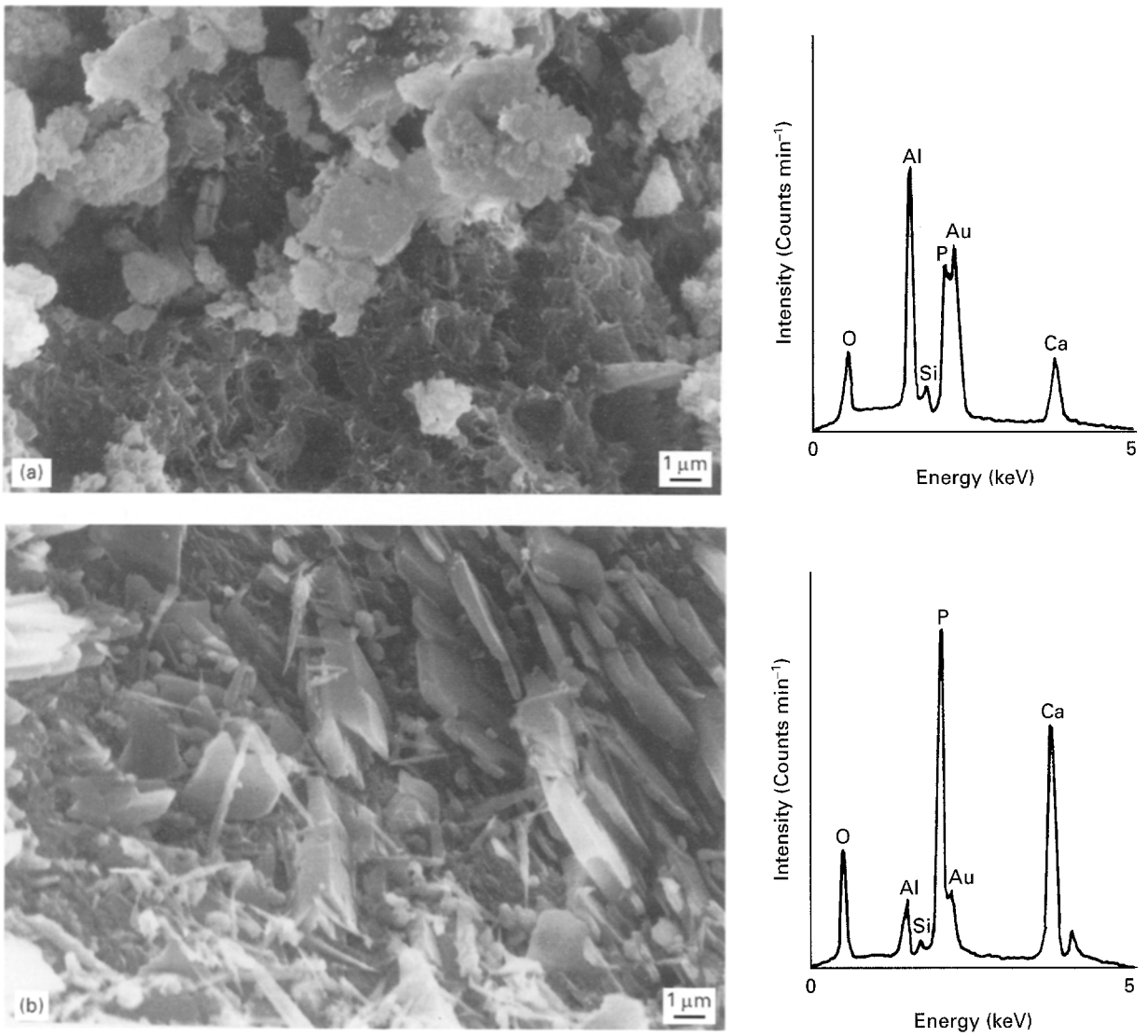

Figure 9 Scanning electron micrographs coupled with EDX for fractured surface of (a) 100 °C and (b) 300 °C autoclaved VPA–RE systems.

and non-reacted C_2AS as minor ones. Although not shown in any figures, the morphological features similar to those of the VPA–RE system were observed from the #80 system. No SEM exploration was made of the G system because the setting of this cement was too fast to pour it into the cylindrical moulds.

Overall, the FT–IR, XRD, and SEM–EDX data conclusively demonstrate that the amorphous and crystal line phase composition of VPA–#80, -RE and -G system cements prepared under atmospheric and hydrothermal conditions depends mainly on the chemical components of cements used as the base reactants and on the temperature. The resulting phase compositions for each base reactant are summarized in Table III as a function of temperature. With regard to the phase transition, in the #80 system, the acid–base reaction between VPA and CA or CA_2 at 25 °C led to the formation of amorphous CCVP salt as the major reaction product, and $Al_2O_3 \cdot xH_2O$ gel as the by-product. The CCVP was favourably converted into amorphous CPPH at a hydrothermal temperature of 100 °C, and concurrently, the $Al_2O_3 \cdot xH_2O$ formed by the phase segregation of CA and CA_2 was transformed into the crystalline γ-AlOOH phase. At 200 °C, the CPPH → crystalline HOAp phase transition seemed to be initiated, and this transition was completed at 300 °C. However, overall there was no clear transition of α-Al_2O_3 phase with temperature in #80. A phase-transition route similar to that of the #80 system was found in the RE system. The strong alkalinity of the C_3S reactant as the major phase of G cement led to the decomposition of unsaturated vinyl groups in the VPA when the VPA and G were mixed at 25 °C. The CPPH → HOAp phase transition and the precipitation of silica gel in the G system occurred at 100 °C. At 300 °C, two components, HOAp and silica gel, become a dominant phase in the cement bodies, while the C_3S reactant is no longer present.

These *in situ* phase transitions and phase-composition changes, and the development of microstructure directly affect the porosity and compressive strength of autoclaved specimens. Table IV compares these factors of the specimens prepared by exposing for 20 h to hydrothermal temperatures of 100, 200, and 300 °C. No determination was made of the porosity and com-

TABLE III Amorphous and crystal-phase compositions for VAP–#80, -RE, and -G cement systems as a function of temperature

System	Temperature (°C)	Major phase	Minor phase
VPA–#80	25	CCVP, $Al_2O_3 \cdot xH_2O$, α-Al_2O_3, CA, CA_2, VPA	–
VPA–#80	100	CPPH, $Al_2O_3 \cdot xH_2O$, α-Al_2O_3, CA, CA_2	γ-AlOOH
VPA–#80	200	CPPH, α-Al_2O_3, γ-AlOOH	HOAp, CA, CA_2, $Al_2O_3 \cdot xH_2O$
VPA–#80	300	HOAp, α-Al_2O_3, γ-AlOOH	CPPH
VPA–RE	25	CCVP, $Al_2O_3 \cdot xH_2O$, CA, C_2AS, VPA	CA_2
VPA–RE	100	CPPH, $Al_2O_3 \cdot xH_2O$, CA, C_2AS	CA_2, γ-AlOOH
VPA–RE	200	CPPH, γ-AlOOH, C_2AS	HOAp, CA, CA_2, $Al_2O_3 \cdot xH_2O$
VPA–RE	300	HOAp, γ-AlOOH, C_2AS	CPPH
VPA–G	25	CPPH, C_3S	–
VPA–G	100	CPPH, C_3S	HOAp, $(SiO_2)_n \cdot xH_2O$
VPA–G	200	CPPH, C_3S	HOAp, $(SiO_2)_n \cdot xH_2O$
VPA–G	300	HOAp, $(SiO_2)_n \cdot xH_2O$	CPPH

TABLE IV Changes in porosity and compresive strength for VPA–#80 and -RE systems as a function of hydrothermal temperatures

System	Hydrothermal temperature (°C)	Porosity (%)	Compressive strength (MPa)
VPA–#80	100	61.7	2.18
VPA–#80	200	79.4	1.39
VPA–#80	300	81.3	0.67
VPA–RE	100	45.2	11.03
VPA–RE	200	49.1	25.60
VPA–RE	300	56.5	8.11

pressive strength of the G specimens because the cement slurry set too quickly after mixing. When the 25 °C made #80 specimens with a porosity of 53.3% and compressive strength of 0.23 MPa were exposed in an autoclave at 100 °C, strength was increased by ≈ 2.5 fold, while the porosity increased to 68.2%. There was a further increase in porosity in the 200 and 300 °C autoclaved specimens, to 79.4% and 81.3%, respectively. As expected, the development of such porous structures produced a serious loss of strength. In contrast although porosity tended to rise with increasing temperature, the RE systems had low values ranging form 45.2–56.5%. Particularly, an interesting fact was that the highest strength of 25.6 MPa in this test series was obtained with the 200 °C autoclaved specimens. However, increasing the temperature to 300 °C caused a retrogression of strength. Therefore, it appears that moderate growth of crystalline HOAp in the amorphous CPPH phase improves the compressive strength, whereas an excessive growth of HOAp crystals results in the loss of strength.

4. Conclusion

In synthesizing calcium phosphate cements (CPC) at 25 °C through the acid–base reaction between vinylphosphonic acid (VPA) and calcium aluminate cement (CAC) or calcium silicate cement (CSC) as the base reactants, the extent of the reactivity between them depended mainly on the CaO mole fraction in the chemical components of base reactants, and the degree of their alkalinities. The high CaO content and strong alkalinity of tricalcium silicate ($3CaO \cdot SiO_2$, C_3S) as the major phase of CSC offered the lowest onset temperature of exothermic reaction with VPA, compared with those of monocalcium aluminate ($CaO \cdot Al_2O_3$, CA) and calcium bialuminate ($CaO \cdot 2Al_2O_3$, CA_2) as the main components of CAC, thereby accounting for the rapid setting behaviour of CPC.

The acid–base reaction between VPA and CAC provided the formation of amorphous calcium-complexed vinylphosphonate (CCVP) salt, which is responsible for strengthening the CPC specimens at 25 °C. Simultaneously, calcium-depleted CA and CA_2 in the CAC caused the precipitation of $Al_2O_3 \cdot xH_2O$ gel as the by-product. The reaction product differed from CCVP was identified in the VPA–CSC system; namely, the susceptibility of unsaturated vinyl groups in VPA to alkali-induced degradation led to the formation of amorphous calcium pyrophosphate hydrates (CPPH) which act to shorten significantly the setting periods of CPC.

In hydrothermal environments, the CCVP and $Al_2O_3 \cdot xH_2O$ phases derived from VPA–CAC systems at 25 °C were transformed, respectively, into the CPPH, and crystalline γ-AlOOH phase at 100 °C. Increasing the temperature to 200 °C led to amorphous CPPH → crystalline hydroxyapatite (HOAp) phase transitions. This transformation in the VPA–CSC system occurred at the relatively low temperature of 100 °C; at 300 °C, and CPPH → HOAp and $Al_2O_3 \cdot xH_2O \rightarrow$ γ-AlOOH phase transitions were completed. Relating such phase compositions and transitions to the development of strength, the highest compressive strength for autoclaved specimens with a porosity of < 50% was obtained from a moderately mixed phase of amorphous CPPH and crystalline HOAp. However, excessive growth of HOAp in the amorphous layers caused the loss of strength.

Acknowledgement

This work was performed under the auspices of the US Department of Energy, Washington, DC under Contract DE-AC02-76CH00016.

References

1. T. SUGAMA and N. R. CARCIELLO, *J. Am. Ceram. Soc.* **74** (1991) 1023.
2. T. SUGAMA, M. ALLAN and J. M. HILL, *ibid.* **75** (1992) 2076.
3. T. SUGAMA and N. R. CARCIELLO, *Cem. Concr. Res.* **25** (1995) 91.
4. *Idem, ibid.* **23** (1993) 1409.
5. J. ELLIS and A. D. WILSON, *J. Mater. Sci. Lett.* **9** (1990) 1058.
6. M. J. O'NEAL, *Anal. Chem.* **36** (1964) 1238.
7. M. G. WYZGOSKI, *J. Appl. Polym. Sci.* **25** (1980) 1455.
8. L. C. THOMAS and R. A. CHITTENDEN, *Spectrochim. Acta.* **26A** (1970) 781.
9. J. ELLIS and A. D. WILSON, *Polym. Int.* **24** (1991) 221.
10. D. E. C. CORBRIDGE, and E. J. Lowe, *J. Chem. Soc.* (1954) 493.
11. E. Z. ARLIDGE, V. C. FARMER, B. D. MITCHELL and W. A. MITCHELL, *J. Appl. Chem.* **13** (1963) 17.
12. T. SUGAMA and N. R. CARCIELLO, *Adv. Cem. Res.* **5** (1993) 31.
13. R. A. NYQUIST and R. O. KAGEL, "Infrared Spectra of Inorganic Compounds" (Academic Press, New York, 1971) p. 95.

Received 31 May 1995
and accepted 2 July 1996